Current Optics and Photonics
Vol. 4, No. 3, June 2020, pp. 221-228

ISSN: 2508-7266(Print) / ISSN: 2508-7274(Online)
DOI: https://doi.org/10.3807/COPP.2020.4.3.221

All-fiber RGB Laser Light Source of Head-up Display System for Automobile Application

Jonggwan Lee[1], Kyungwon Kim[1], Seong-Jin Son[2], Bok Hyeon Kim[1], and Nan Ei Yu[1]*

[1]Advanced Photonics Research Institute, Gwangju Institute of Science and Technology, Gwangju 61005, Korea
[2]Department of Physics and Photon Science, Gwangju Institute of Science and Technology, Gwangju 61005, Korea

(Received December 11, 2019 : revised February 7, 2020 : accepted April 20, 2020)

We developed an all-fiber RGB laser light source module for application in an automobile head-up display. It is based on laser diodes and an optical fiber combiner that substantially enhances the flexibility of configuration and stability against harsh working conditions for automobiles. We coupled 13 laser diodes with optical fibers and merged them into a single output with a beam combiner device. Red (R), green (G), and blue (B) laser sources were employed to produce primary colors that were mixed into a white light output. An optical output power of approximately 1.5 W was achieved, and the color balance of the output lights was assessed based on the CIE 1931 color space. The optical output power was shown to be stable for over 160 h within an optical fluctuation of less than 0.27%.

Keywords : Laser projection display, Optical system design
OCIS codes : (120.4820) Optical systems; (140.7300) Visible lasers; (220.2945) Illumination design; (220.4830) Systems design; (330.1730) Colorimetry

I. INTRODUCTION

As a cutting-edge transportation technology, vehicular automation has attracted considerable attention in the past decade. Systems to help drivers while driving are called advanced driver assistance systems (ADAS). An ADAS system can support advanced safety and convenient driving through electronic stability control, antilock braking systems, lane departure warnings, adaptive cruise control, etc. Owing to the development of sensor and image processing technology, the market volume for such systems is rapidly growing and is expected to expand further. It is expected that highly automated cars will be able to drive by themselves on highways, and door-to-door fully automated driving is also expected to be possible in the near future [1-3].

In comparison with conventional driver assistance systems such as global positioning system (GPS) navigation systems, an ADAS needs to deliver a larger amount of information to a driver. Although automobile display systems are now widely used, their screen size is too small for ADAS to supply enough information to a driver. Moreover, it is difficult to maintain the attention of drivers with conventional displays for automobiles because they are located outside the line of sight of drivers. This can cause distractions for the driver, which can lead to high-risk situations. For these reasons, Head-up display (HUD) systems have recently been highlighted as a next-generation display for automobiles [4]. A HUD is a transparent display located right in front of the driver's line of sight through the windshield as a virtual image. It presents information without requiring users to avert their eyes to the side and allows them to keep looking ahead, which reduces distraction and substantially enhances safety in driving. HUD technology has a promising outlook, and several approaches have been recently reported to improve its performance, such as the application of

*Corresponding author: neyu@gist.ac.kr, ORCID 0000-0001-5078-8842
Color versions of one or more of the figures in this paper are available online.

waveguide optics [5], micro lens array optics [6], and the exploitation of noble polymer-based liquid crystals [7].

A typical HUD system employs a projection scheme, requiring a backlight combined with a picture generation unit and an optical system [8]. For the light source, most commercialized HUD systems utilize light-emitting diodes (LEDs), and their properties have been greatly improved. However, LED sources have several shortcomings and are constrained by them. For example, the possible display size is constrained by low brightness of the optical output. Even though high-power LED have been commercialized, the spectral properties are not sufficient to cover all the requirements of advanced HUD. High-power LEDs still have variations in color temperature and aging effect.

As an alternative, laser light sources are expected to overcome the drawbacks of LED sources. They have higher brightness, thus allowing larger display, better contrast, and more monochromatic output which has a wider representable color range [9, 10]. They also have a longer lifetime and higher energy efficiency. However, despite these advantages, laser sources have not been commercialized in a HUD system because of problems such as speckle noise and eye safety issues [11, 12].

In this report, we present an all-optical fiber-based laser light source module. Laser diodes were coupled with a set of focusing lenses and optical fibers. Light from the diodes goes through the fiber to be combined into a single output fiber with an optical fiber combiner device. R, G, and B colored laser diodes were used as primary color light sources to achieve over 500 mW optical power of each color on the output fiber terminal. This output yield is high enough to produce a brightness of approximately 20,000 cd/m^2 and a large virtual display. We also assessed the color balance of the output light by measuring the power density spectrum in the frequency domain and analysis them based on the CIE 1931 color space [13, 14]. It reveals the representable color gamut and the power ratio required to produce white light output, which is 1:0.57:0.41 for RGB.

II. RESULTS AND DISCUSSION

A typical white-light source made by mixing primary color laser sources utilizes dichroic mirrors. These mirrors selectively reflect the light to combine the three separated beams. However, this setup requires deliberate alignment, whereas the automobile application environment usually includes harsh mechanical vibration and acceleration. To overcome this difficult usage environment, we used an optical fiber combiner [15] to mix and deliver the light source (see Fig. 1). This configuration highly enhances robustness to mechanical impact. Moreover, the fiber-based system allows a flexible arrangement of optical devices and other pieces of apparatus. These features enable the module to tolerate vibration in moving cars and make them suitable for practical applications.

In detail, 13 red, green, and blue laser diodes were used to yield white light illumination at the output end. Seven of them were red laser diodes as they have lower individual output power compared to green and blue ones, while the remainder consisted of three blue and three green laser diodes. Laser lights from diodes are individually coupled into the cores of the input optical fibers with core/clad diameters of 105/125 μm by using a set of microlenses. The input optical fibers were made using silica materials and the numerical apertures (NAs) of the fibers were 0.22 in a step index profile.

To combine the 13 separated input laser beams and make a single output at the output fiber terminal, the input fibers were bundled and fused tapered to have a slowly varying outer diameter curvature by using a tapered fusion machine equipped with a micro gas torch, as shown in Fig. 2 (see Refs. [15] and [16]). Then, the fused fiber bundle

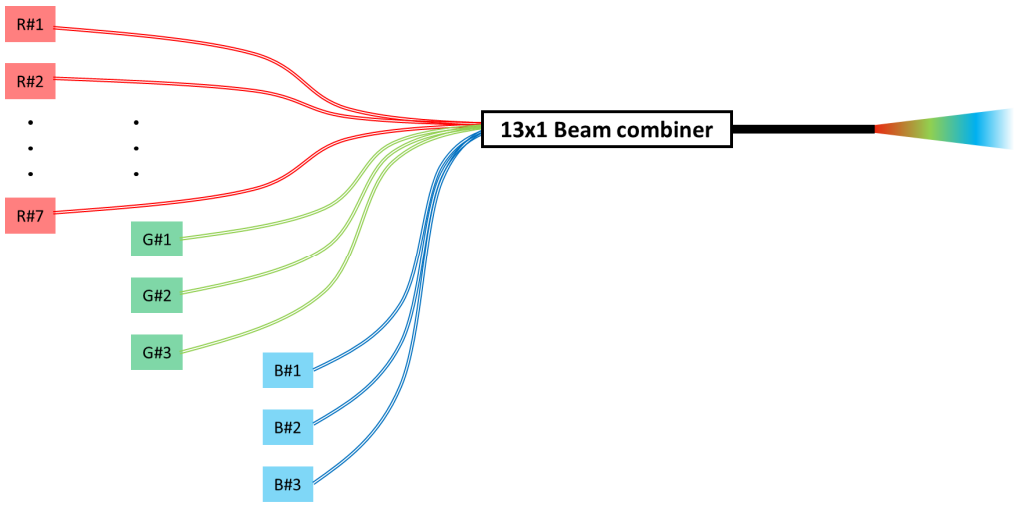

FIG. 1. Schematic diagram of 13 × 1 all-fiber laser light source module.

was cleaved at a tapered region and spliced with a single output fiber with a large core/clad diameter of 400/440 μm. For the output fiber, low-index polymer-coated silica fiber was used. It should be noted that the low-index polymer was used as a clad material and the NA of the fiber was 0.46.

Bundling and fusing of fiber ends combine light from several input fibers into a single output fiber. To minimize structural insertion loss, one should consider the beam product parameter (BPP) given by the product of the core diameter (D) and numerical aperture ($NA = \sqrt{n_{core}^2 - n_{clad}^2}$) of the optical fiber. The beam product parameter (BPP), $D \times NA$, of the output fiber should be larger than the sum of the BPPs of the input fibers. In this manner, a 13 × 1 fiber coupler that combines 13 inputs into a single output was designed and fabricated. This fiber combiner module has over 75% power transmission between the 13 separate input channels and the output terminal for RGB laser light, thus enabling a power emission of 1.5 W at the output terminal. These components are packaged in a box case to serve as a modularized appliance (see Table 1 and Fig. 3).

In 2014, a compact RGB fiber pigtailed laser module for pico-projector display was introduced [17]. Designed housing and epoxy were used to make the fiber bundle; however, we used a fused tapering technology at high temperature [15, 18]. The fabricated fiber bundle has the physical properties of the fusion, and a single output fiber with the light pipe was used.

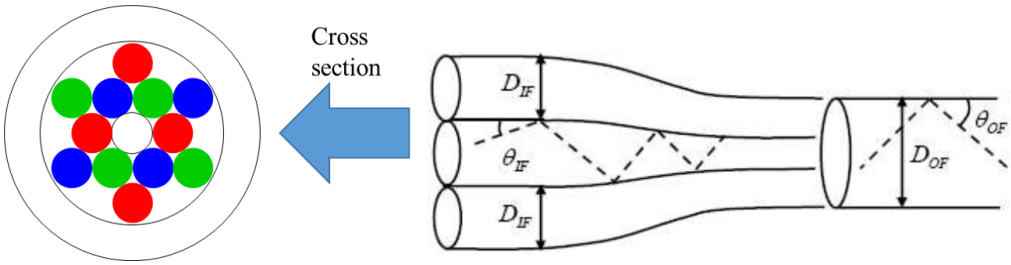

FIG. 2. Diagram of the (13 × 1) combiner for optical coupling of the LDs. D_{IF}: diameter of input beam, D_{OF}: diameter of output fiber, Θ_{IF}: input angle of the beam, Θ_{OF} : output angle of the beam.

TABLE 1. Main specifications of the RGB laser module

	Red	Green	Blue
Center frequency (nm)	638	519	459
Power (mW)	>500		
Fiber	[Input] Core diameter: 105 (um) NA: 0.22 Multi-mode fiber		[Output] Core diameter: 400 (um) NA: 0.46 Multi-mode fiber
Size (mm)	W 120 × H 60 × L 200 (fiber is not included)		

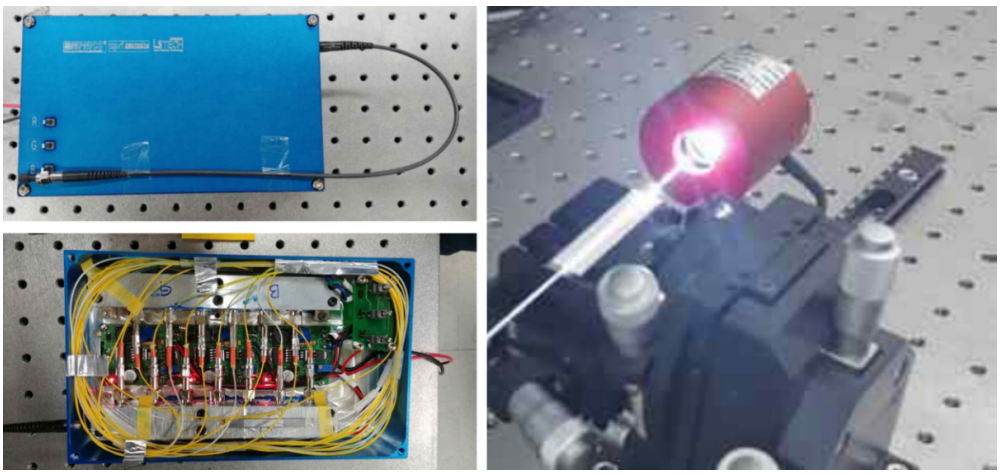

FIG. 3. Packaged light source module and its inside (left); light emission from output terminal (right).

The radiant flux spectrum of the output light was multiplied by the standard photopic luminosity function and integrated over the visible wavelength region to yield the total luminous flux of the light source. The developed light source module with a power output of 500 mW for each color band yields a total luminous flux of 341.5 lumens. This corresponds to a luminance of 23,717 cd/m^2, assuming a 45-inch virtual screen at a distance of 4 m. Considering that typical displays for computers emit only a few hundreds of cd/m^2, the achieved luminance output largely exceeds the required specification for the HUD system. This has the potential to produce larger displays, even when allowing for the relatively low reflectivity of a transparent screen.

The spatial beam profiles of the R, G, B, and white light output beams are shown in Fig. 4. The light emission from the laser diodes has an elongated rectangular geometry which elongates the beam output. These oblong beam profiles are

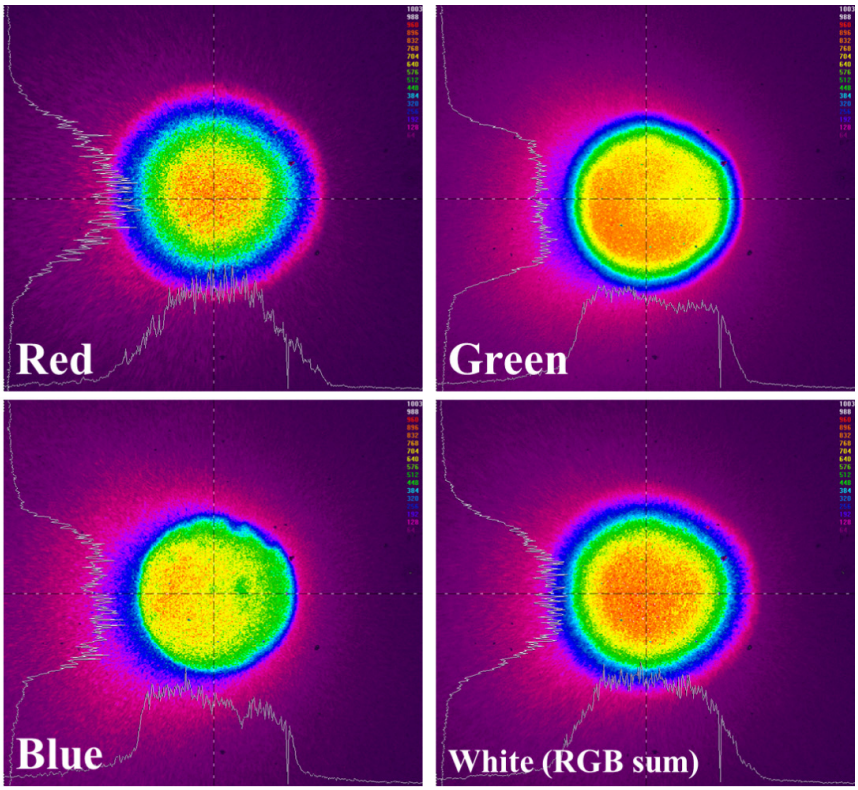

FIG. 4. Spatial profiles of each color output.

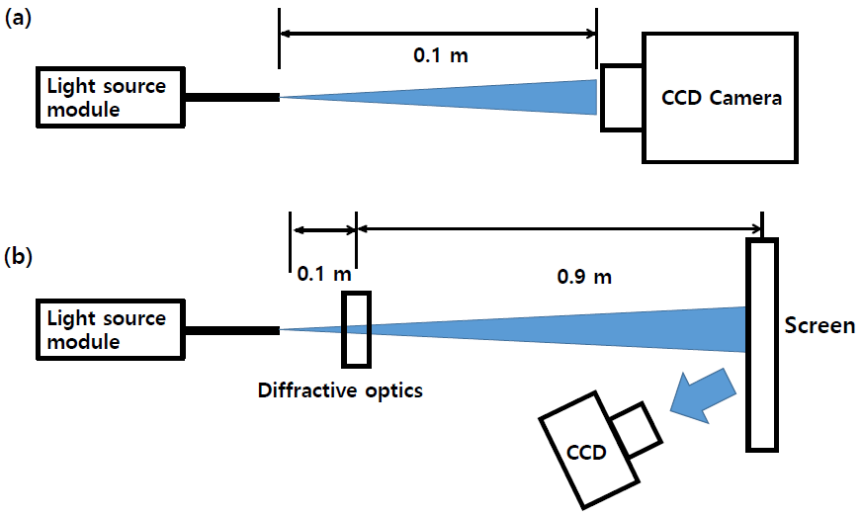

FIG. 5. Schematic diagram of experimental setups to acquire: (a) spatial profile, (b) Speckle noise pattern of the output light.

converted to circular shapes by using cylindrical lenses for effective transmission through optical fiber. The angular distribution of the light flux in the far field was captured by a beam diagnostic camera (Coherent® LaserCam II), for which the experimental layout is depicted in Fig. 5(a). As the energy density of the output beam was considerably higher than the CCD saturation limit, neutral density filters were employed to attenuate the output illuminance without harming the original beam shape.

Each RGB output beam showed a circular beam shape; while the red beam had a well-fitted Gaussian beam shape, blue and green beam profiles seemed to have the intensity profiles similar to circular top-hat. For practical applications in an HUD system, these output beams can be shaped with a fly-eye lens array to have a uniform square flat-top profile, which is suitable as a backlight for projection displays. Figure 6 shows the radiant flux spectra of the output beam in the frequency domain for RGB color bands and two different white lights, as explained below. The spectra were obtained in a geometry similar to the spatial profile measurement, with a visible-range spectrometer (Avantes® Avaspec-DDDD-2-USB2) instead of a camera. No filtering was used in the spectrum measurement to prevent spectral distortion induced by a filter. The center frequencies acquired from the Gaussian best fit of RGB spectra were 638, 519, and 459 nm, respectively, with full-width half-maximum bandwidths of 4.2, 5.1, and 3.7 nm, respectively.

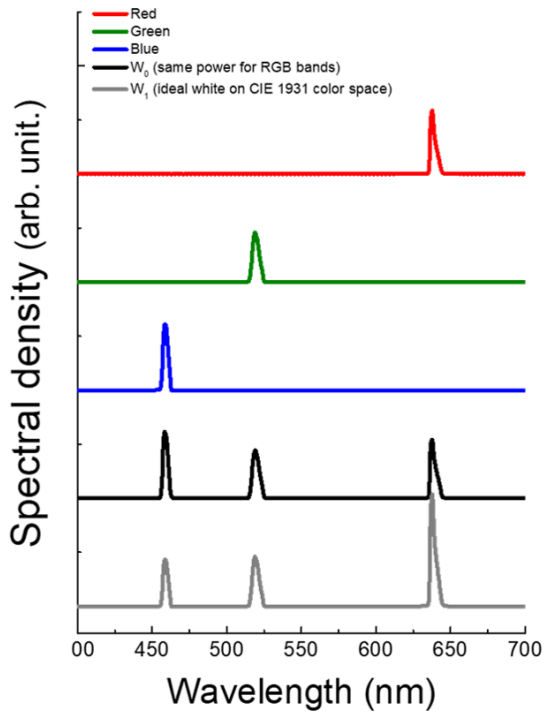

FIG. 6. Frequency domain spectrum of the output light. W_0: mixture of RGB bands having equal power, W_1: mixture of RGB bands having adjusted power ratio to yield white light (R:G:B = 1.00:0.57:0.41).

The CIE 1931 color space was used to quantitatively assess the color balance of the output light. In CIE 1931 theory, the power density spectra of the output lights $L(\lambda)$ (mW/nm) are multiplied by dimensionless color matching functions $\bar{x}(\lambda)$, $\bar{y}(\lambda)$ and $\bar{z}(\lambda)$, and integrated over the visible range $\lambda \in [380,780]$ to yield tristimulus values X, Y and Z [13, 19].

$$X = \int_{visible} L(\lambda)\bar{x}(\lambda)d\lambda$$
$$Y = \int_{visible} L(\lambda)\bar{y}(\lambda)d\lambda \quad (1)$$
$$Z = \int_{visible} L(\lambda)\bar{z}(\lambda)d\lambda.$$

Then, the color coordinates (x, y) on the color space can be readily derived from these parameters. They are defined as follows:

$$x = \frac{X}{X+Y+Z}$$
$$y = \frac{Y}{X+Y+Z}. \quad (2)$$

The color coordinates corresponding to the R, G, and B output spectra are listed in Table 2 and illustrated in Fig. 7. Each RGB monochromatic output is located at the edge of the visible color gamut, thus allowing a far wider representable color range than other sources such as traditional lamps or LEDs. In addition to showing the coordinates for the RGB outputs, the figure shows two different mixtures. One of them, denoted by W_0, has equal output power for each RGB band. As shown in Fig. 7, the color coordinates corresponding to this light deviate from the desired white point. Based on colorimetry theory [20, 21], we calculated the optimal power ratio between RGB bands to yield ideal white light, denoted by W_1. The power ratio was found to be R:G:B = 1.00:0.57:0.41.

When intended for use as an automobile accessory, the module should be verified in terms of compatibility and durability for an automobile environment. For example, a lab-made PCB driver circuit board that regulates current and voltage applied to laser diodes is specifically designed to have compatible electromagnetic radiation characteristics. It requires an environment guaranteed to be without interference from any other appliances in the car and is certified by a third-party testing company. Moreover, durability at high temperature and humidity, which is also a critical feature of a commercialized car accessory, has been tested and verified according to the Telcordia GR-1221 standard qualifications. It showed successful operation after 1,000 h of aging at 85°C/85% R.H. condition, and also after 85 recurrent thermal cycles between -40°C and 85°C (2 h dwell time, 1 h transfer time).

TABLE 2. Color coordinates corresponding to R/G/B and two different white lights. W_0: mixture of RGB bands having equal power, W_1: mixture of RGB bands having adjusted power ratio to yield white light (R:G:B = 1.00:0.57:0.41)

Color	*x*	*y*
Red	0.7048	0.2934
Green	0.1277	0.8272
Blue	0.1380	0.0616
W_0	0.2318	0.2876
W_1	0.3127	0.3291

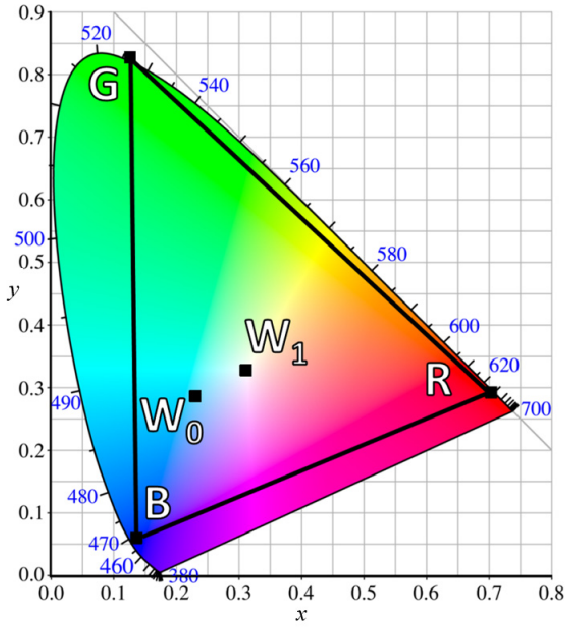

FIG. 7. Color coordinates of five different output lights displayed in the CIE 1931 color space. The triangle connecting R/G/B points illustrates the representable color gamut of the light source module.

Functional stability is one of the most important features that should be verified before practical application. We checked the operational stability of the module (see Fig. 8) by leaving it turned on and fully operational over a long time period. It maintained its output illuminance compared to the initial output after 10,000 min (approximately 166 h) of operation. The fluctuation in output illuminance was 0.27% compared to the average output over the operating time, which promises performance stability over several days of operation.

Speckle noise is one of the major technological obstacles to a laser as a projection light source [22]. The surface of a screen for HUD is very rough on the scale of the visible light wavelength; therefore, incident light would be irregularly reflected from the screen surface. The reflected beams interfere with each other, causing granular noise on the projected vision, which is called speckle noise. This

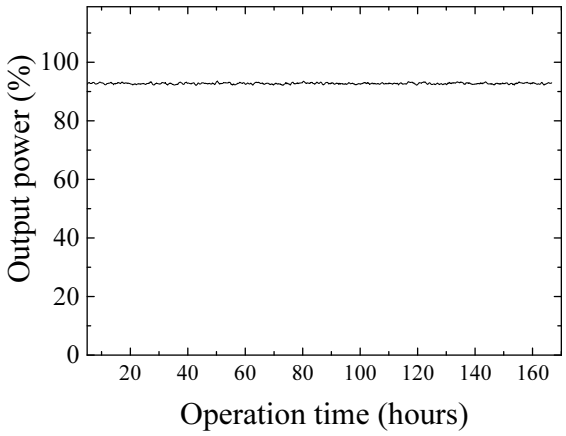

FIG. 8. Output stability of long-term operational condition.

noise occurs inherently and degrades the quality of an image, especially when it is delivered by coherent light. Because the coherent nature of laser light is vulnerable to speckle noise, speckle noise suppression is usually addressed by intentionally reducing the coherence of the light, such as linewidth broadening or polarization diversification. In our case, we employed oscillating diffuser optics to handle speckle [22-25]. We used a diffuser plate with a 6° diffusion angle and a 10 mm diameter clear aperture. By oscillating at the frequency of approximately 180 Hz (peak-to-peak amplitude of 400 μm), the plate attenuates the speckle noise of the laser output. To evaluate the extent of speckle noise suppression, we measured the speckle contrast from the projection image of the output light according to a standardized speckle quantification process [26].

Light emission from the module was illuminated on a white screen made of paper. The differential optics, if used, are located between the beam output and the screen (see Fig. 5(b)). We captured the speckle patterns occurring on the screen with a CCD camera (Viewworks® VM-11M5). The experimental conditions were set to 50 ms of exposure time, 2^{12} steps of dynamic range, and 3.2 mm aperture size, which were chosen to mimic the response of the human eye to a typical image projection. The speckle pattern that appears on the image can be represented as a qualitative parameter via mathematical pixel-by-pixel calculation. The speckle contrast ratio (C) is defined by the standard deviation of the intensity divided by the average intensity. In the following equation, parameter *I* denotes the intensity measured by a single pixel of the array detector, and the angle bracket symbol <> describes the ensemble average of the argument.

$$C = \frac{\sqrt{\langle I^2 \rangle - \langle I \rangle^2}}{\langle I \rangle}. \tag{3}$$

The speckle images taken for eight different conditions (R/G/B/W operational modes with/without diffractive optics) are shown in Fig. 9. The speckle ratio of the RGB source

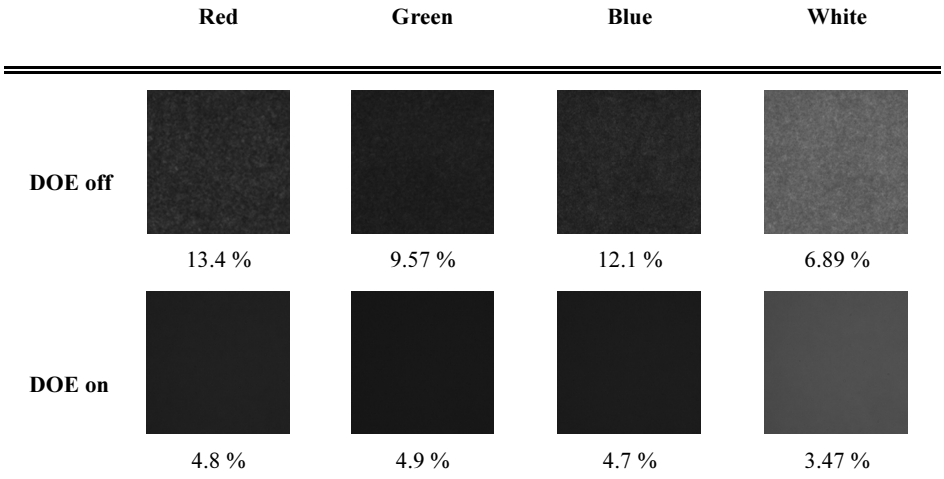

FIG. 9. Summarized speckle patterns and contrast. Diffractive optical elements (DOEs) were proven to reduce speckle noise by half.

before applying diffractive optics, which varied with color, is approximately 10%. With the help of DOEs, the speckle ratio is reduced by approximately half, or under 5% for each of the R, G, and B monochromatic outputs. In the case of white light output, the speckle ratio is intrinsically lower than that of RGB light, as its polychromatic nature decreases the coherence length and hinders optical interference. It shows a speckle ratio of approximately 7%, which is reduced by half using diffractive optics. The previously reported speckle perception limit is approximately 4% [26], which means that humans cannot recognize speckle contrast less than this. The employment of DOE, which reduces speckle noise from 10 to 5% (R/G/B separately) and 7 to 3.5% (white), prevents noise disturbance and, therefore, play a crucial role in the application of laser projection display.

III. CONCLUSION

In summary, we have developed a novel light source module for a laser projection display based on laser diodes and fiber optics. The system successfully enhanced the mechanical stability and flexibility of the component arrangement. Over 1.5 W of optical output power was achieved for HUD applications. This is useful for providing a 45-inch virtual display of luminance greater than 20k cd/m^2 with an HD level of resolution. The required power ratio to achieve an ideal white balance was calculated to be R:G:B = 1.00:0.57:0.41. Diffractive optics components were employed to reduce the speckle noise ratio by half. This light module can be commercialized in the near future for automotive aftermarkets as part of HUD systems.

ACKNOWLEDGMENT

We would like to acknowledge our colleagues at MPNICS Co. and LS Tech. Co. in Gwangju, Korea for their efforts on development and cooperation. This work was partially supported by GIST Research Institute (GRI) grant funded by the GIST. This research is also supported by the Ministry of Trade, Industry, and Energy (MOTIE) under the "Public Institution Linked Regional Industry Development Program", and "Global professional technology development (No. 20003777)," South Korea.

REFERENCES

1. M. Bibuli, M. Caccia, and L. Lapierre, "Path-following algorithms and experiments for an autonomous surface vehicle," IFAC Proc. Vol. **7**, 81-86 (2007).
2. Z. Sun, G. Bebis, and R. Miller, "On-road vehicle detection: A review," IEEE Trans. Pattern Anal. Mach. Intell. **28**, 694-711 (2006).
3. K. Bengler, K. Dietmayer, B. Farber, M. Maurer, C. Stiller, and H. Winner, "Three decades of driver assistance systems: Review and future perspectives," IEEE Intell. Transp. Syst. Mag. **6**, 6-22 (2014).
4. Y.-C. Liu and M.-H. Wen, "Comparison of head-up display (HUD) vs. head-down display (HDD): Driving performance of commercial vehicle operators in Taiwan," Int. J. Hum. Comput. Stud. **61**, 679-697 (2004).
5. C. M. Bigler, P.-A. Blanche, and K. Sarma, "Holographic waveguide heads-up display for longitudinal image magnification and pupil expansion," Appl. Opt. **57**, 2007-2013 (2018).
6. M. K. Hedili, M. O. Freeman, and H. Urey, "Microlens array-based high-gain screen design for direct projection head-up displays," Appl. Opt. **52**, 1351-1357 (2013).
7. S.-L. Hou, W.-K. Choi, and G.-D. J. Su, "Ultra-bright heads-up displays using a method of projected color images by combination of LEDs and polymer-dispersed liquid crystals," J. Disp. Technol. **10**, 228-234 (2014).
8. J. Ma, "Advanced MEMS-based technologies and displays," Displays **37**, 2-10 (2015).
9. K. Blankenbach and E. Buckley, "Perceptual effects of laser-Based HUDs," J. Disp. Technol. **8**, 194-197 (2012).

10. K. Yamamoto, "Laser display technologies and their applications," Adv. Opt. Technol, **1**, 483-488 (2012).
11. S.-J. Son, D.-K. Ko, and N. E. Yu, "Study of an optical device based on a quasi-phase-matching method for speckle noise reduction for laser display," J. Korean Phys. Soc. **69**, 756-761 (2016).
12. N. E. Yu, J. W. Choi, H. Kang, D.-K. Ko, S.-H. Fu, J.-W. Liou, A. H. Kung, H. J. Choi, B. J. Kim, M. Cha, and L.-H. Peng, "Speckle noise reduction on a laser projection display via a broadband green light source," Opt. Express **22**, 3547-3556 (2014).
13. T. Smith and J. Guild, "The C.I.E. colorimetric standards and their use," Trans. Opt. Soc. **33**, 73-134 (1931).
14. K. Hieda, T. Maruyama, T. Takesako, and F. Narusawa, "New method suitable for measuring chromaticity and photometric quantity of laser displays," Opt. Rev. **25**, 175-180 (2018).
15. LS Tech, "Pump Combiners (n+1)×1," (LSTECH, Published: 1 July 2014) http://lstech.kr/?page_id=113 (Accessed date: 11 December 2019).
16. B. Wang and E. Mies, "Review of fabrication techniques for fused fiber components fiber lasers," Proc. SPIE **7195**, 71950A-1 (2009).
17. M. Ide, S. Fukaya, K. Yoda, and M. Suzuki, "Compact multiple laser beam scanning module for high-resolution pico-projector applications using a fiber bundle combiner," Proc. SPIE **9005**, 9005F (2014).
18. S. H. Lee, K. H. Kim, H. S. Yang, S. Y. Cho, S. J. Kim, M. K. Park, and J. H. Lee, "Fabrication and output characteristics of an (18+1)×1 polarization-maintaining pump and signal combiner for high-power fiber laser," Korean J. Opt. Photon. **30**, 187-192 (2019).
19. W. D. Wright, "A re-determination of the trichromatic coefficients of the spectral colours," Trans. Opt. Soc. **30**, 141-164 (1929).
20. N. I. Speranskaya, "Determination of spectrum color coordinates for twenty-seven normal observers," Opt. Spectrosc. **7**, 424-428 (1959).
21. S. Wen, "Design of relative primary luminances for four-primary displays," Displays **26**, 171-176 (2005).
22. M. N. Akram and X. Chen, "Speckle reduction methods in laser-based picture projectors," Opt. Rev. **23**, 108-120 (2016).
23. P.-H. Yao, C.-H. Chen, and C.-H. Chen, "Low speckle laser illuminated projection system with a vibrating diffractive beam shaper," Opt. Express **20**, 16552-16566 (2012).
24. A. Lapchuk, V. Yurlov, G. A. Pashkevich, A. Prygun, A. A. Kryuchyn, and S. Shylo, "Impact of aberrations on speckle suppression efficiency on moving a DOE inside the optical system," Displays **43**, 1-8 (2016).
25. K. Kasazumi, Y. Kitaoka, K. Mizuuchi, and K. Yamamoto, "A practical laser projector with new illumination optics for reduction of speckle noise," Jpn. J. Appl. Phys. **43**, 5904-5906 (2004).
26. S. Roelandt, Y. Meuret, G. Craggs, G. Verschaffelt, P. Janssens, and H. Thienpont, "Standardized speckle measurement method matched to human speckle perception in laser projection systems," Opt. Express **20**, 8770-8783 (2012).